Journal of Building Engineering 31 (2020) 101360

Contents lists available at ScienceDirect

Journal of Building Engineering

journal homepage: http://www.elsevier.com/locate/jobe

Experimental study of seismic behaviour of renovated masonry structures after removing walls and seismic retrofitting

Fang-fang Wei [a], You-hua Zhu [a], Jun Yu [a, *], Yong-quan Wang [b]

[a] College of Civil & Transportation Engineering, Hohai University, Nanjing, 210098, China
[b] School of Architecture Engineering, Nanjing Institute of Technology, Nanjing, 211167, China

ARTICLE INFO

Keywords:
Seismic behaviour
Masonry structures
Renovation
Seismic retrofitting
Strengthening

ABSTRACT

Structural renovation is an economic choice to expand space of existing masonry buildings. To this end, removing bearing walls and seismic strengthening are required in engineering practice in seismic-prone areas. Therefore, in the paper three 1/2-scale two-bay two-storey planar masonry structures, consisting of one original structure and two structures with proposed renovation schemes, were fabricated and tested under cyclic loading. The original structure consisted of brick masonry units, ring beams, and tie-columns. The first renovated structure was designed by removing two bearing walls at the ground storey, adding two short-width shear walls, and enlarging the beam sections. The second renovated structure was achieved by removing one wall in the ground storey, enlarging the sections of confined beams and columns to form a single-bay frame, and retrofitting the adjacent wall with reinforcement layers and polymer mortar. Results indicate that all three specimens demonstrated hysteretic behaviour with pinching phenomenon. Energy dissipation capacity of the two renovated structures were both higher than that of the original structure prior to 1% drift, in particular for the first renovation scheme. In comparison, the second renovation scheme more evidently improved structural resistance, but it made the ultimate deformation capacity smaller than the original structure because the stiffness of the renovated ground story much larger than that of the second story resulted in failure concentration at the 2nd floor. Thus, it is more economic to make the lateral stiffness of the two storeys compatible during the design of renovation and strengthening.

1. Introduction

With the development of economy, some old masonry structures cannot meet the living requirements due to small spans and outdated architecture layouts etc. Consequently, it is necessary to renovate old masonry buildings to expand the space and rearrange the layouts. In China, the typical renovation scheme is removing bearing walls and constructing reinforced concrete (RC) or steel plate-masonry composite underpinning beams to sustain the gravity load from upper storeys; otherwise it is possible to cause progressive collapse [1–3]. The RC underpinning beams are categorized into single-beam, double-beam and frame underpinning. In the first scheme, a single underpinning beam is directly constructed at the top of the wall to be removed, whereas in the second scheme, two beams were constructed at both sides of the top of the walls to be removed. These single-beam and double-beam underpinning schemes requires constructing underpinning beams and demolishing the masonry walls almost at the same time, and thus these two schemes affect the use of storeys below the underpinned storey during renovation. Therefore, they are more used to underpin the ground storey. In the third scheme, steel plates are used to connect part of masonry walls to form steel-masonry composite underpinning beams and framed columns with tie bars and constructional glue. The remaining masonry walls are then demolished. The composite beams are attached with U-shaped steel plates, and the composite columns are enclosed by steel plates. This scheme requires short construction period, but short of codified design method [4].

Seismic retrofitting is required for masonry walls if demands are improved either due to code update or considering the amplification effect of masonry walls on floor acceleration [5], or cracking and minor damage have occurred subjected to previous earthquakes. The typical seismic retrofitting approaches to improve the tensile resistance and energy absorption include applying reinforcement and mor-

* Corresponding author.
E-mail address: yujun@hhu.edu.cn (J. Yu).

https://doi.org/10.1016/j.jobe.2020.101360
Received 11 January 2020; Received in revised form 9 March 2020; Accepted 17 March 2020
Available online 23 March 2020
2352-7102/© 2020 Elsevier Ltd. All rights reserved.

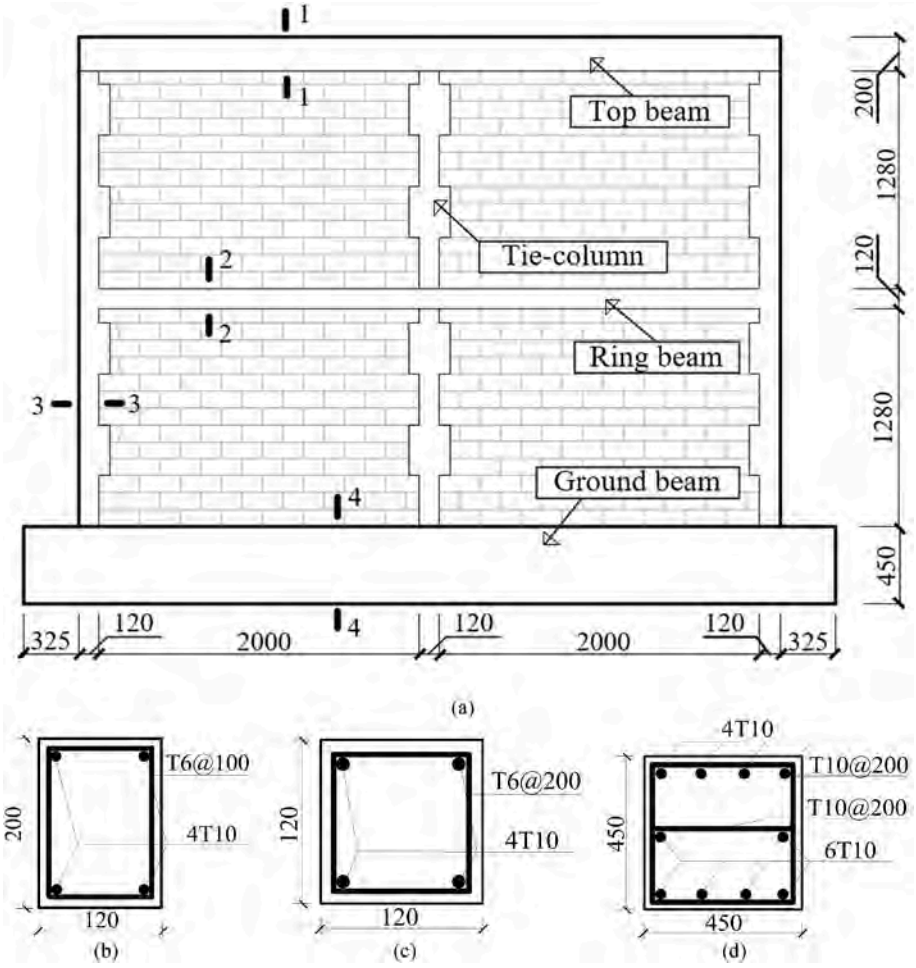

Fig. 1. Geometric dimensions and detailing of the specimen W1 (unit: mm): (a) Overall scheme; (b) Section 1-1; (c) Section 2-2(3-3); (d) Section 4-4.

tar layer, attaching steel plates and fibre reinforced polymer sheets etc. Due to the lightweight and the ease in use, externally attaching carbon fibre reinforced polymers (CFRP) and/or glass fibre reinforced polymers (GFRP) is one of the most effective methods in strengthening recently. Can [6], Capozucca [7] and Gams et al. [8] investigated the seismic behaviour of masonry walls after retrofitted by CFRP and GFRP and found that: 1) the application of external bonded CFRP and GFRP are unable to enhance the load capacity but can improve the deformation capacity and ductility; 2) the compressive strength of masonry units affects the strengthening of CFRP strips; and 3) the failure of retrofitted walls is caused by debonding of coating, resulting in sharp degradation of resistance and stiffness. The efficiency of seismic retrofit measure using Near-Surface Mounted (NSM) CFRP strips was experimentally investigated, and the results suggested that NSM CFRP retrofit technique is a minimally-invasive option for seismic strengthening of unreinforced masonry walls to resist out-of-plane lateral forces [9].

Besides fibre reinforced polymers, other materials with high tensile strength and ductility are also applied at the surfaces of masonry walls to improve their structural performance against lateral loads. Shabdin et al. [10] presented that strengthening masonry walls using textile reinforced mortar (TRM) can extremely improve diagonal load carrying capacity and deformation capacity, especially for the walls strengthened on both side surfaces. Xu et al. [11] found that attaching reinforcement layer and cement mortar at both sides of masonry walls is able to improve lateral bearing capacity and integrity of the walls. Lin et al. [12,13] employed engineered cementitious composite (ECC) shotcrete to strengthen masonry walls and found that ECC shotcrete is able to effectively improve the in-plane and out-of-plane bearing capacity as well as ductility of masonry walls. Maaheri et al. [14] used RC layer to retrofit single-face of masonry walls, and numerically pointed out increasing thickness of RC layer is able to improve shear capacity of retrofitted walls but reduce ductility, and the reinforcement ratio of RC layer has little effect on the shear capacity of retrofitted walls. Khan et al. [15] experimentally and numerically investigated the in-plane strength of masonry panels strengthened with geotextile. The result demonstrated that strengthening increases load carrying capacity, stiffness and deformation capacity.

Moreover, the current researches on the renovation of existing masonry structures with underpinning schemes focus more on the construction methods and techniques, and only a few are about the structural behaviour of underpinning members under vertical load [16–18]. For example, Zhang X et al. [16] designed nine specimens of mansory wall underpinned by double-beams and invesitgate the effects of underpinning beam depth and arrangement of longitudinal reinforcement on the structural behaviour and failure modes under vertical load. The results indicated that with increasing underpinning beam depth, the failure mode of the underpinned structure changed from punching failure at the interface between the masonry and the beams to the diagonal compression or local bearing failure.

In summary, the studies on seismic retrofitting of masonry walls are mainly based on single wall panel under cyclic loading, and the research on renovated masonry walls are focused on the structural behaviour under gravity load. However, the seismic behaviour of entire renovated masonry structures is rarely reported. Therefore, in this paper three 1/2 scaled two-bay two-storey planar masonry structures,

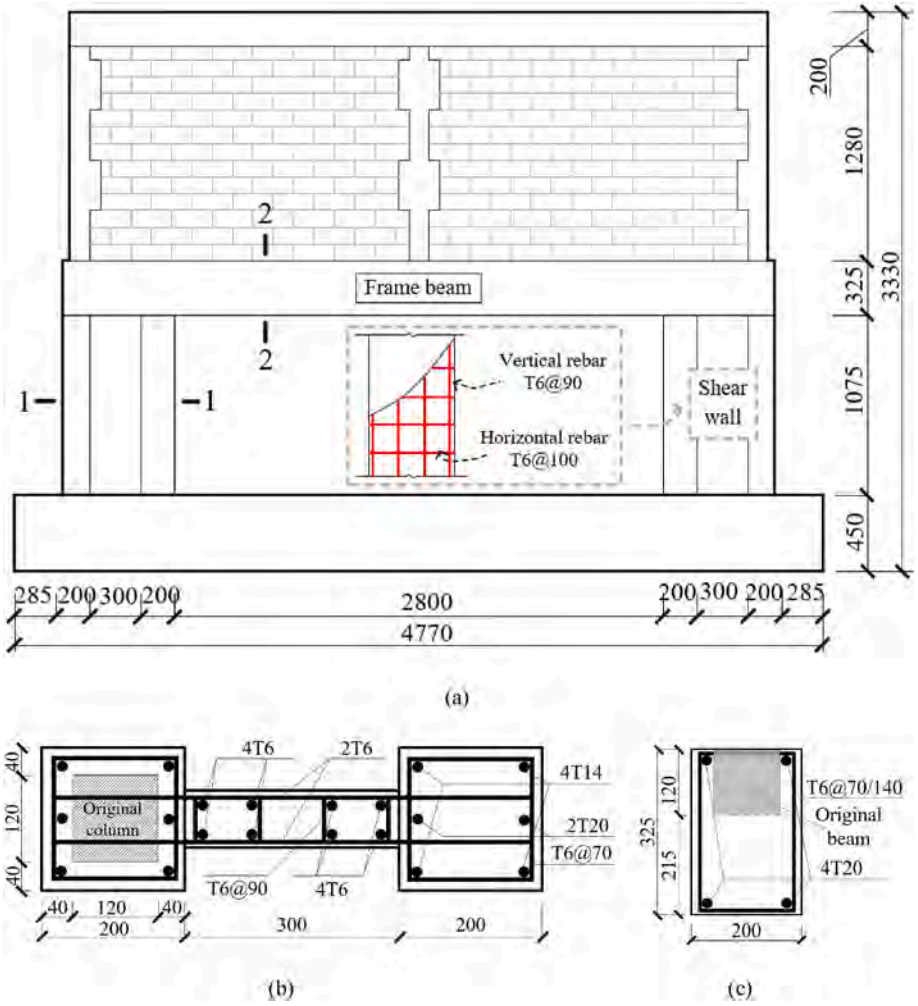

Fig. 2. Geometric dimensions and detailing of the specimen W2 (unit: mm): (a) Overall scheme; (b) Section 1-1; (c) Section 2-2.

including one original structure and two renovated structures designed with proposed renovation schemes, were tested under cyclic loading. The effect of the proposed renovation schemes on seismic behaviour was investigated in terms of failure modes, crack pattern, hysteretic curves and energy dissipation capacity etc. Finally, the suggestions for the renovation schemes regarding seismic performance are provided.

2. Experimental program

2.1. Specimen design

In this experimental programme, three 1/2 scaled two-bay two-storey masonry specimens were fabricated. One specimen (namely, W1) represented an original structure and the other two specimens (namely, W2 and W3) corresponded to renovated masonry structures with the renovation schemes proposed by the authors. As seen in Fig. 1, W1 consisted of brick masonry units, ring beams and tie-columns. Note that the tie-columns were constructed with finger joints to ensure the integrity of the masonry wall panels and surrounding RC frames. As shown in Fig. 2, W2 represents the case that the masonry frame was renovated with two bearing walls at the ground storey removed and retrofitted by two short-width shear walls and underpinning beams. In specimen W3, as seen in Fig. 3, one wall was removed and the sections of the confined beams and columns were enlarged to form a frame. The other wall in the ground storey was retrofitted by reinforcement layer and polymer mortar, corresponding to the case with removing a single bearing wall. For the three specimens, the compressive cubic strength of concrete was 35.7 MPa and the average compressive strength of masonry bricks was 12.1 MPa.

The prototype of the specimens was a 6-storey confined masonry structure with a storey height of 2.8 m, a bay and span length of 4 m, which was designed in accordance with Chinese code for design of masonry structures [19] and Chinese code for seismic design of buildings [20]. The cross sections of both tie-columns and ring beams were 240 mm in square. The superimposed dead load acting at the typical storeys and the roof was 2.06 kN/m^2 and 4 kN/m^2, respectively. The live load for all the storeys was 2 kN/m^2. The building was located in the region with site category one and seismic design intensity of 7°, corresponding to peak ground acceleration of 0.1 g.

2.1.1. Specimen W1

The geometric dimensions and reinforcement detailing of specimen W1 are shown in Fig. 1. The span length was 2000 mm and the storey height was 1400 mm. The cross sections of the tie-columns and ring beams were 120 mm in square, and the ones for top beam were 120 mm wide and 200 mm deep. To facilitate anchoring the wall specimen and provide solid foundation, an additional ground beam with cross-section of 450 mm square was made. The concrete cover for all the members was 15 mm. Both the top and bottom longitudinal reinforcing bars in the ring beams were 2T10 with stirrups of T6@200 mm, and the longitudinal rebars in the columns were 4T10. In the plastic hinge regions of 250 mm in tie-columns, the stirrups

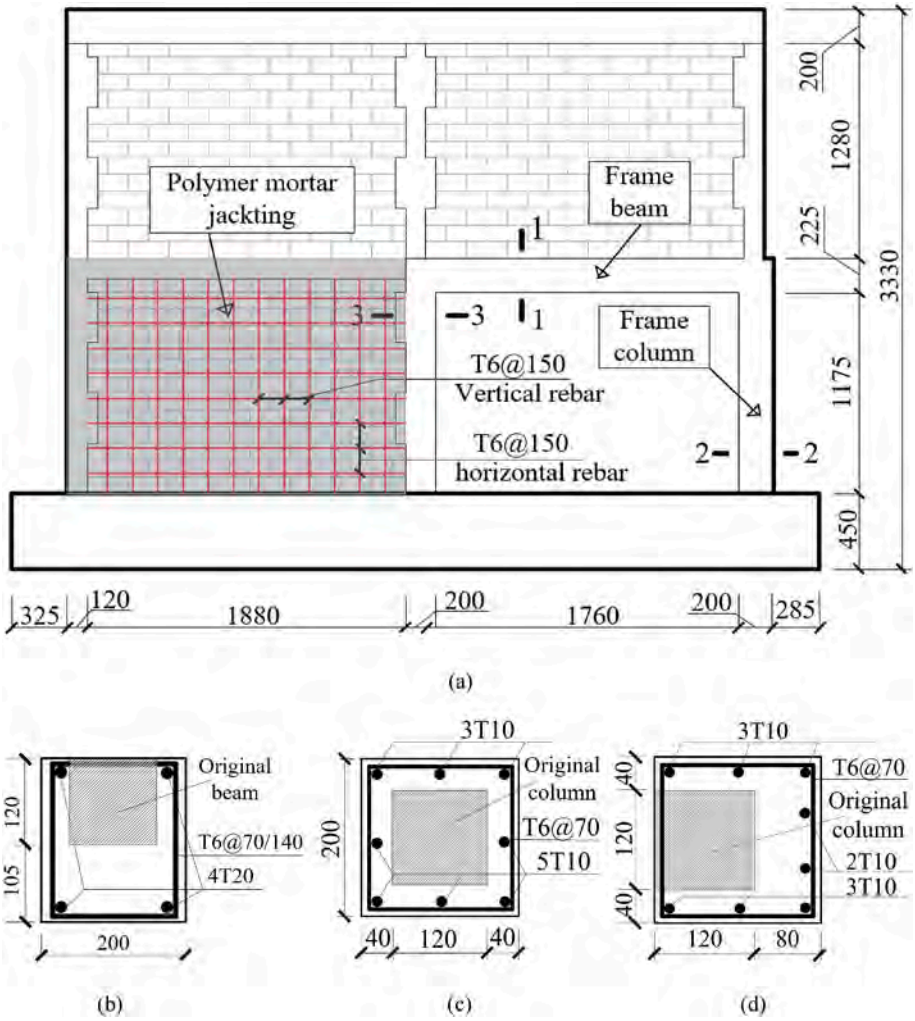

Fig. 3. Geometric dimensions and detailing of the specimen W3 (unit: mm): (a) Overall scheme; (b) Section 1-1; (c) Section 2-2; (d) Section 3-3.

Table 1
Material properties of steel reinforcement.

Steel bar	Diameter (mm)	Yield strength (MPa)	Ultimate strength (MPa)	Elastic modulus (× 10^5MPa)
T 6	6	493.7	677.0	1.89
T10	10	467.9	629.4	2.00
T14	14	485.5	650.8	2.10
T20	20	490.7	685.7	2.00

were T6 with center-to-center spacing of 100 mm, and in the middle span of them, the stirrups spacing was 200 mm.

2.1.2. Specimen W2

To renovate the original masonry structure, two ground-storey walls and middle tie-column were removed. To ensure the load carrying capacity and the seismic resistance, during the renovation design the main procedure was as follow:

1) The cross sections of the ring beam were enlarged using grouting material, and the enlarged geometric dimension is shown in Fig. 2 (c). Outside the original ring beam, longitudinal reinforcing bars of 4T20 were used with stirrups of T6@70/140 mm, and the eventual cross section was 200 mm wide and 325 mm deep. The compressive strength of the grouting material was 70.4 MPa, based on the tests of the standard cubes. The material properties of steel reinforcement are listed in Table .1.
2) Two RC shear walls with small width were added to increase the lateral stiffness of the ground storey as shown in Fig. 2(a). Each shear wall consisted of two boundary columns (functioning as flanges) and a web, in which one boundary column was fabricated by enlarging the section of the original tie-column and placing additional longitudinal reinforcing bars of 4T14 and 2T20. The eventual geometric dimension of the boundary columns was 200 mm square, and the cross section of the wall web was 300 mm wide and 120 mm thick, as shown in Fig. 2(b). In the web, two orthogonal layers of steel reinforcement with diameter of 6 mm were placed with the vertical and horizontal spacing of 90 mm and 100 mm, respectively, as highlighted in Fig. 2 (a). 2.1.3 Specimen W3

In the second renovation scheme, one span of the wall was removed to construct a frame and the wall in the adjacent span was strengthened with additional reinforcement layer and polymer mortar to provide lateral stiffness of the ground storey, as shown in Fig. 3(a). The detailing of W3 is as follows:

1) The cross section of the frame columns was 200 mm square, which was enlarged on top of a tie-column, as shown in Fig. 3(c) and (d), and the frame beam was 200 mm wide and 225 mm deep, which was enlarged on top of a ring beam, as shown in Fig. 3(b). The longitudinal reinforcement bars of frame columns was 8T10, and the stirrups were T6@70 mm. Both the top and bottom

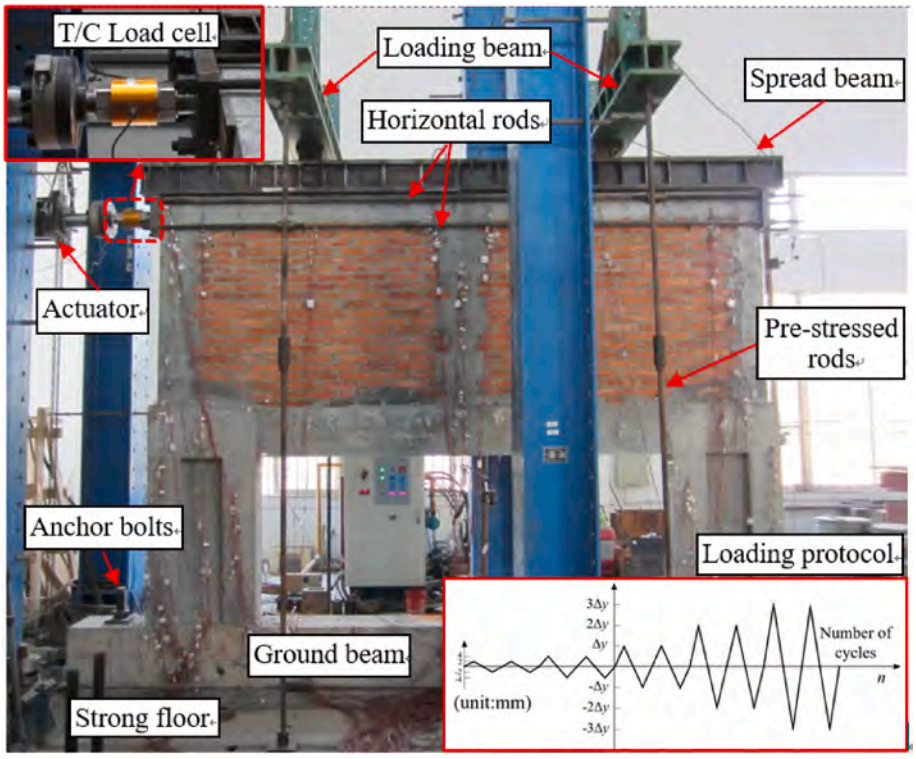

Fig. 4. Test set-up of cyclic testing.

longitudinal reinforcement bars in the frame beam were 2T20 with stirrups of T6@70/140 mm.

2) At both sides of the masonry wall, a reinforcement layer with vertical and horizontal bars T6@150 mm was installed and then a polymer mortar jacketing with thickness of 30 mm was applied. The compressive strength of polymer mortar is 39.6 MPa.

2.2. Test setup and instrumentation

Fig. 4 shows the cyclic test set-up. Each specimen was anchored onto the strong floor with the anchor bolts through the two ends of the ground beam. In the horizontal direction, a servo-controlled hydraulic actuator was installed onto the reaction wall and attached to the top of each specimen. In vertical direction, two rods were pre-stressed between the strong floor and a loading beam at each bay, which was supported by a spread beam seated onto the top beam. To ensure the vertical load not affecting the horizontal displacement of the masonry wall, a roller support was inserted between the loading beam and the spread beam.

A tension/compression load cell with measuring capacity of 500 kN, as highlighted in Fig. 4, was installed between the actuator and the loading plate to measure the applied horizontal load. To measure the story drift, two displacement transducers with measuring capacity of 200 mm were respectively installed at the right end of the top beam and the fist-floor beam, and one displacement transducer with measuring capacity of 25 mm to measure the movement of the ground beam if any. During the test, the data recording frequency was 0.5 Hz.

2.3. Testing procedure

In the test program, the vertical load corresponding to 60 kN/m was applied at the top beam in both spans, corresponding to the total vertical load of 261.6 kN. The horizontal loading protocol with displacement-controlled method was adopted in the test, as shown in the inset of Fig. 4. Two fully reversed cycles were imposed at each displacement level. The displacement was applied with an increment of every 2 mm until the cracking of specimen and the slope of load-displacement significantly decreased, at which the corresponding displacement was estimated as Δ_y. Since then, the displacement was imposed with an increment of every estimated Δ_y until failure, corresponding to the horizontal load decreased to 85% peak load.

3. Experimental results

3.1. Global response and local failure modes

3.1.1. Specimen W1

In the initial loading stage, the envelope curve of the load-displacement was linear, as shown in Fig. 5(a). The first horizontal crack occurred at the bottom of left tie-column in the 2nd storey during the first 9 mm displacement cycle, corresponding to the lateral load of 168.5 kN. During the first 14 mm displacement cycle, the horizontal cracks occurred at the top and bottom of the exterior tie-columns of the ground storey. More subsequent cracks were observed under the cyclic loading as indicated in Fig. 6(a). During the first 44 mm displacement cycle, primary cracks occurred at the 2nd storey walls, and the crushing of bricks was observed as well as the X-shaped shear cracks of the 2nd storey middle tie-column as illustrated in Fig. 6(b) and (c), resulting in severe deformation of the structure, corresponding to the load of around 311 kN. In the following loading, it was found that at the displacement of 51 mm, the structural resistance has dropped to around 196 kN, much less than 85% the peak load, and for the sake of safety, the test was terminated.

3.1.2. Specimen W2

After applying the specified vertical load of 261.6 kN, no cracks were observed in the ground storey beams, demonstrating that the renovation with two I-shaped RC shear walls and strengthened beam by section enlargement met the requirements for service limit state. Then the horizontal load was cyclically imposed and the horizontal load-displacement curve of W2 is shown in Fig. 5(b). In the first 8 mm

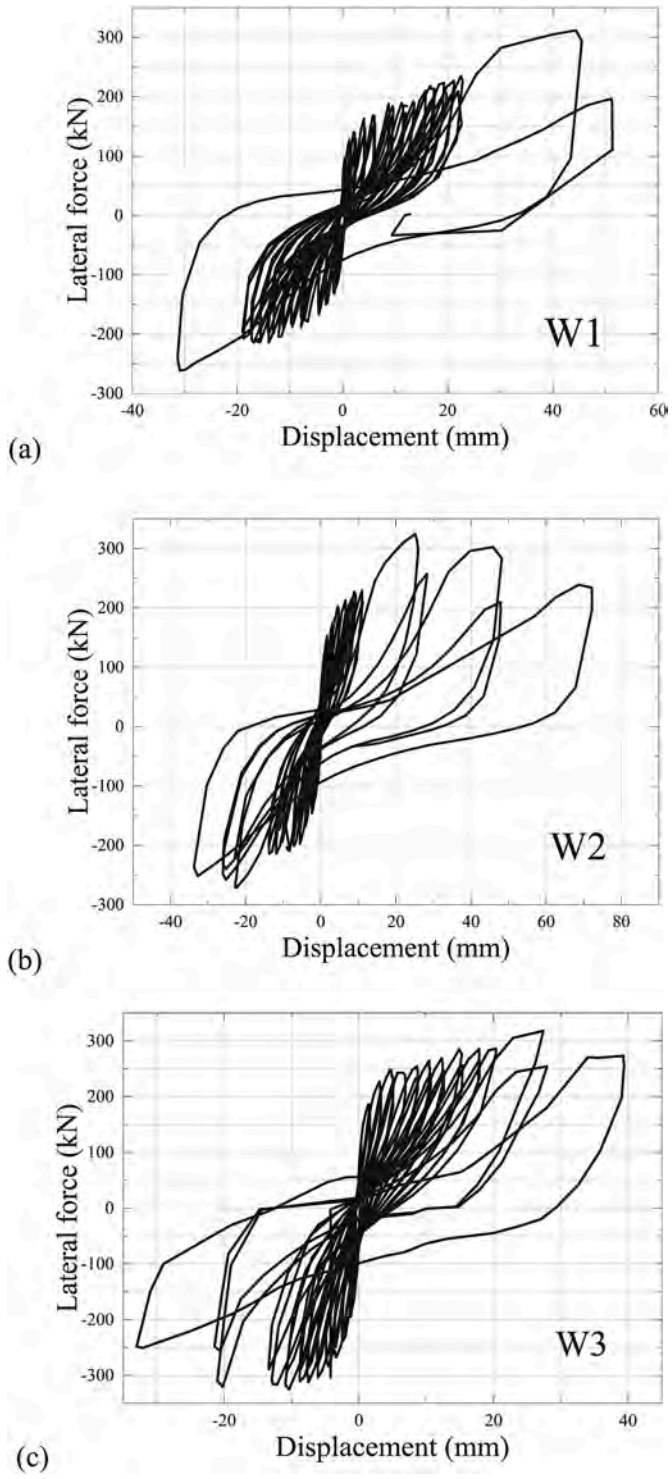

Fig. 5. Hysterisis curves of three specimens: (a) Specimen W1; (b) Specimen W2; (c) Specimen W3.

displacement cycle, the first horizontal crack occurred at the RC shear walls and the boundary columns in the ground storey. Flexural cracks were observed at the middle span of the ground storey beam during the first 10 mm displacement cycle, and more subsequent cracks occurred at the boundary columns of the RC shear walls as shown in Fig. 7(a). During the 12 mm displacement cycle, horizontal cracks appeared at the exterior tie-columns in the 2nd floor. The peak load of 324.34 kN was attained at the displacement of 25.19 mm. Inclined cracks were observed at the top of the side tie-columns and the upper left corner of the left masonry wall on the 2nd floor during the first 32 mm displacement cycle. The primary inclined cracks of the 2nd storey masonry walls extended in the 48 mm displacement cycle, and the crushing of brick was observed as indicated in Fig. 7(b). During the 64 mm displacement cycle, the X-shaped diagonal cracks occurred at the 2nd storey middle tie-column, causing sharp degradation of structural stiffness, and the lateral load was decreased to 244 kN, less than 85% of the peak load. The test was then terminated.

3.1.3. Specimen W3

After applying the specified vertical load of 261.6 kN, no cracks were observed as well, suggesting the current renovation scheme of constructing one-span frame and one-span reinforced masonry wall was able to meet the requirements of the service limit state. Then the horizontal load was cyclically imposed and the horizontal load-displacement curve of W3 is shown in Fig. 5(c). During the first 6 mm displacement cycle, the inclined cracks appeared at the top of tie-columns and masonry walls in the 2nd storey. The horizontal cracks occurred at the top and bottom end of the ground storey frame columns as well as the bottom end of the right tie-column of the 2nd floor in the 8 mm displacement cycle. The horizontal cracks developed inwards the tie-columns as the displacement increased, and more inclined cracks were observed at the 2nd storey masonry walls. In the positive phase of the first 14 mm displacement cycle, the inclined crack was observed at the lower right corner of the right wall in the 2nd storey as well as at the polymer mortar jacketing in the ground storey, as shown in Fig. 8(c). The lateral load reached the peak value at the displacement of 32 mm, and the primary cracks of the two wall panels in the 2nd storey were connected, as shown in Fig. 8(a), causing the degradation of structural resistance. During the 44 mm displacement cycle, the X-shaped diagonal cracks occurred at the 2nd storey middle tie-column (see Fig. 8(b)), and the primary cracks widened, resulting in severe reduction of structural resistance. Consequently, the horizontal load was decreased to less than 85% of the peak load, and the test was terminated.

3.2. Hysteresis behaviour and envelope curves

All the three specimens demonstrate hysteretic behaviour with pinching phenomenon, as shown in Fig. 5(a), (b) and (c). The pinching of hysteresis loops, indicating reduced energy dissipation, is because lateral displacement occurred in conjunction with the opening and closing of cracks in the masonry walls and tie-columns, which consumed smaller energy compared to yielding of reinforcement. Under the successive cycles of a specified displacement level, both stiffness and structural resistance degraded, indicating the damage of concrete, masonry bricks, reinforcement and bed joints. Moreover, the positive phase and the negative phase of the hysteretic curves are not symmetric because loading was controlled in accordance with the displacement of the actuator, and in fact the elongation of the horizontal rods along the 2nd storey beam made the specimen displacing in pulling (i.e., the negative displacement) less than that in pushing (i.e., the positive displacement) at each displacement cycle.

The comparison of the envelope curves as shown in Fig. 9 demonstrates that the renovation scheme for W3, including section enlargement of beams and columns as well as polymer mortar jacketing with reinforcement layer for the shear wall, increased the structural resistance from the displacement of around 2 mm–28 mm in both positive and negative phase with maximum enhancement up to 120 kN at the displacement of −12mm. Moreover, the renovation scheme of W2, including section enlargement of beams and adding two short width shear walls at the ground storey, also greatly enhanced structural resistance with maximum improvement of around 80 kN at the displacement of 25 mm. This suggests that these renovation measures were very beneficial to increase structural resistance although all the three

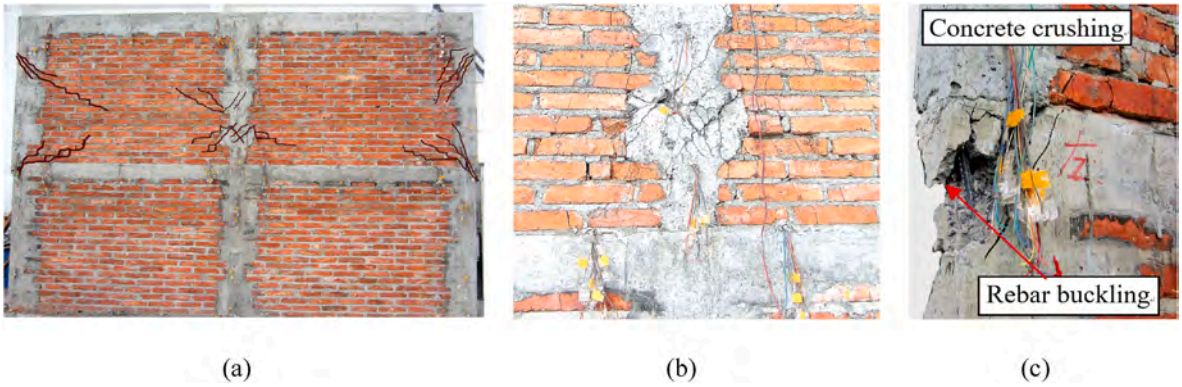

Fig. 6. Failure modes of original mansonry structure: (a) Primary cracks of W1; (b) diagonal cracks of middle tie-column in the 2nd floor; (c) concrete crushing and rebar buckling in the bottom of tie-column in the 2nd floor.

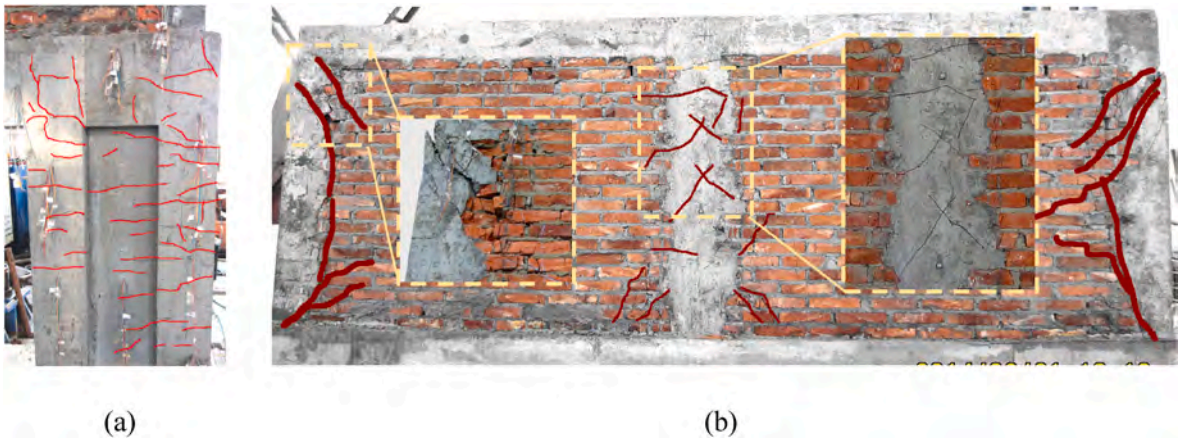

Fig. 7. Failure modes of specimen W2: (a) Horizontal cracks of RC shear walls; (b) Primary cracks of W2 and crushing of masonry unit.

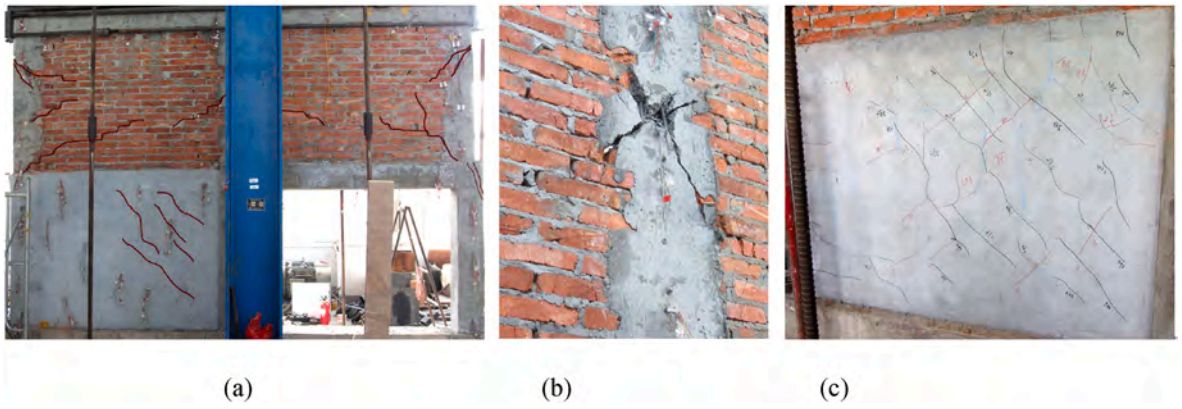

Fig. 8. Failure modes of specimen W3: (a) Primary cracks of W3; (b) Digonal cracks of middle tie-column in the 2nd floor; (c) Cracks of polymer mortar jacketing.

specimens reached the similar ultimate resistance in the positive phase.

On the other hand, the comparison of the positive phase envelope curves indicates that both the post-peak deformation capacity of W2 and W3 significantly exceeded that of W1, in particular, for W2, and the post-peak stiffness of W2 and W3 were smaller than that of W1. That is, both W2 and W3 failed in a more ductile manner than W1 after the peak resistance.

3.3. Summary of structural resistance and displacement

The critical states of the seismic behaviour of the specimens are represented by three main events: first cracking, peak load, and failure. The lateral loads and corresponding displacements of the aforementioned events in the positive phase are shown in Table 2, where Δ_c, Δ_u, Δ_f are the displacements corresponding to first cracking, peak load and failure, respectively. It can be seen that the cracking load of W2 and W3 are larger than that of W1, indicating that the renovated structures are more superior in resisting frequent earthquakes of which the design criteria are bearing capacity and allowed elastic deformation in accordance with Chinese code for seismic design of buildings [20].

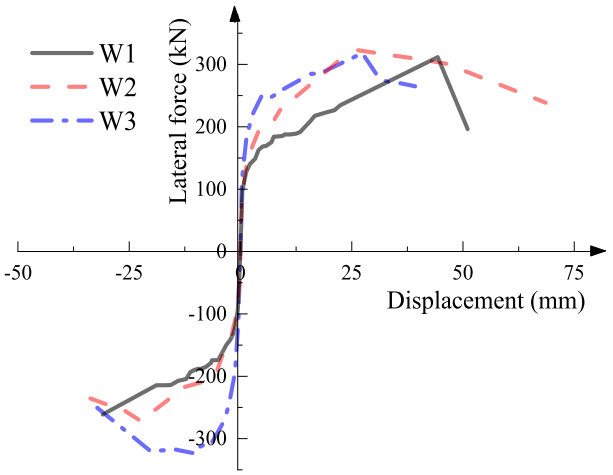

Fig. 9. Envelope curves of masonry structures.

Table 2
Critical load and displacement in loading history.

Specimen	Cracking load and displacement		Ultimate load and displacement		Δ_f
	P_c (kN)	Δ_c (mm)	P_u (kN)	Δ_u (mm)	(mm)
W1	168.50	8.82	311.69	44.37	51.25
W2	212.45	6.63	324.34	25.19	55.56
W3	243.10	5.75	318.02	27.4	39.28

3.4. Degradation of lateral stiffness

The lateral stiffness of the wall specimens is evaluated as the peak-to-peak stiffness of the force-displacement relationship [21]. It is calculated as the slope of the line joining the positive and negative peak loads at a given displacement cycle. Fig. 10(a) illustrates the stiffness of the three specimens degraded with imposing larger lateral displacement Δ, which is normalized by the height H of the top beam axis with respect to the top surface of the ground beam to show global drift. The initial structural stiffness (i.e. K_{max}) of W3 was twice that of W1 and W2. The structural stiffness of the three specimens sharply reduced in the first 6 mm displacement (i.e. Δ/H = 0.2%) and kept decreasing as the drift increased.

Fig. 10(b) demonstrates the stiffness ratio of the second cycle to the first cycle at a given displacement was around 0.85 to 0.95 for three specimens prior to Δ/H = 0.6%, indicating that constant-amplitude cyclic loading caused in-cycle stiffness degradation due to damage accumulation. However, after Δ/H = 0.6%, further increasing displacement exacerbated the in-cycle stiffness degradation. For example, at Δ/H = 1.0%, the in-cycle stiffness degradation was less than 0.8. This suggests that the cyclic loading involving large nonlinear displacement of the structures accelerated the damage accumulation. The variation of in-cycle stiffness ratio of W2 at large displacement ranging from Δ/H = 1.0%–1.7% was evaluated by just two data, which could be affected by the measurement accuracy, but the overall trend of in-cycle stiffness degradation from Δ/H = 0.6%–1.7% was decreasing with increasing deformation.

3.5. Energy dissipation capacity

The energy dissipation capacity of each loading cycle is computed as the area enclosed within the hysteresis loop S_{EBFCE}, as indicated in Fig. 11. Moreover, the energy dissipation capacity can be evaluated by the equivalent viscous damping coefficient h_e [21], using $h_e = S_{EBFCE}/2\pi(S_{AOE} + S_{DOF})$, where S_{AOE} and S_{DOF} are areas within ΔAOE and ΔDOF as shown in Fig. 11. Fig. 12 illustrates that h_e basically kept increasing with imposing larger global drift Δ/H. It is seen that h_e of W3 was slightly larger than that of W1 for Δ/H between 0.5% and 1.0%, and from Δ/H of 1.0%–1.4%, h_e of W1 and W3 was almost identical, indicating that the renovation scheme for W3 ensured similar energy dissipation capacity to the one of original frame W1. Moreover, when Δ/H between 0.5% and 1.1%, the energy dissipation capacity of W2 was larger than that of W1, because the initial

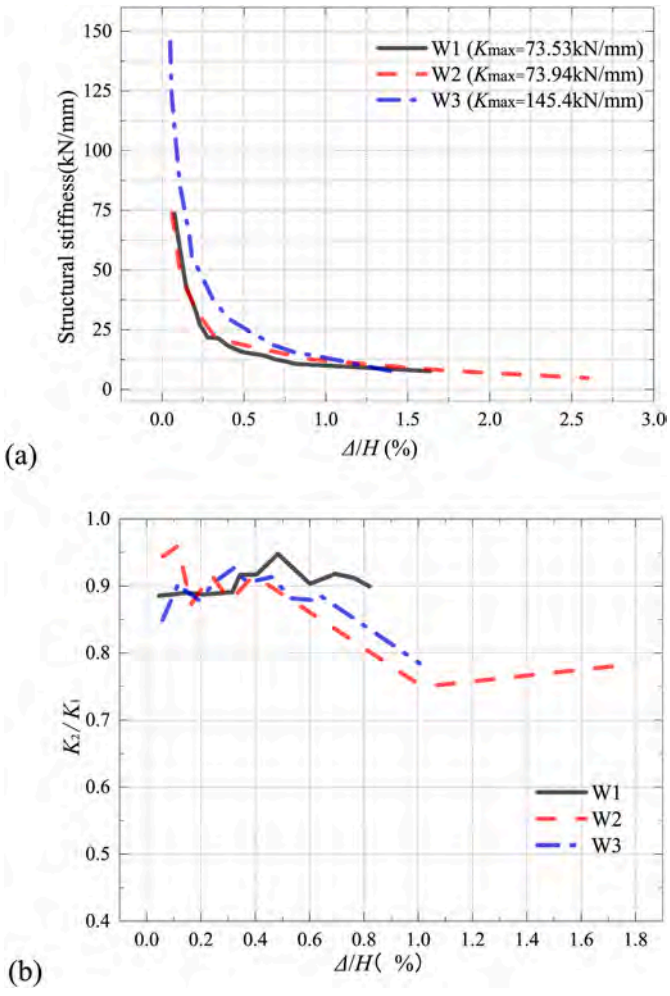

Fig. 10. Comparison of stiffness degradation of masonry structures: (a) Stiffness of the first displacement cycle; (b) Stiffness ratio of the first to the second cycle at a given displacement (H = 2780 mm).

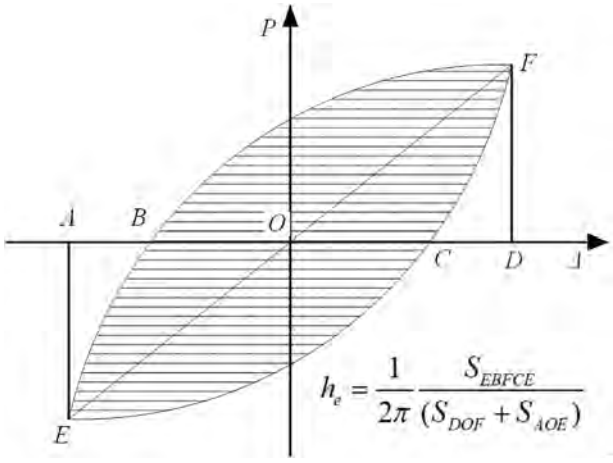

Fig. 11. Approach to calculate the equivalent coefficient of damping.

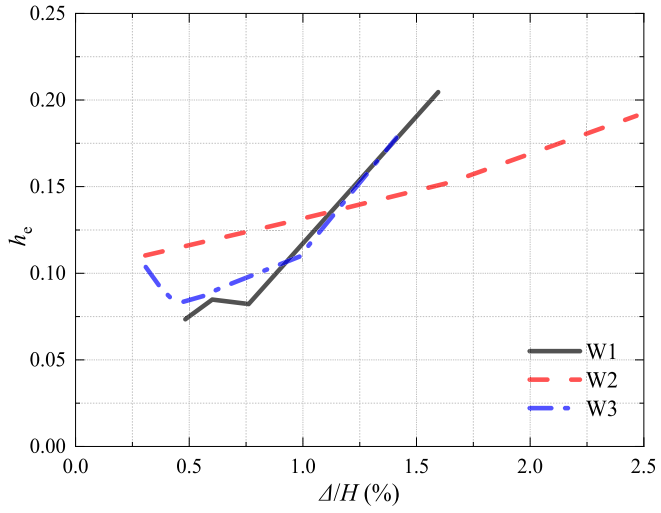

Fig. 12. Comparison of damping coefficients of masonry structures (H = 2780 mm).

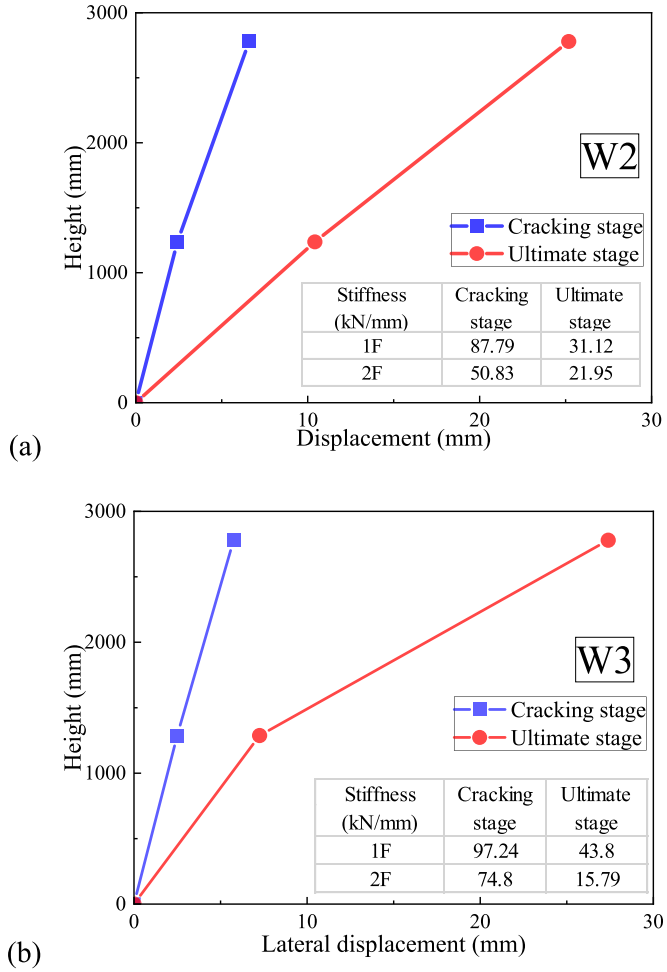

Fig. 13. Lateral deformation of storey at critical stages: (a) Specimen W2; (b) Specimen W3.

damage of W2 occurred at the short width shear walls, which was more ductile compared with masonry walls in W1. However, with further increasing the lateral displacement, the severe cracking and local failure became more evident at the un-strengthened 2nd storey of W2, as shown in Fig. 7, resulting in its energy dissipation capacity smaller than that of W1 at the same lateral displacement. This reflects that the un-strengthened 2nd storey eclipsed the energy dissipation capacity contributed by the renovated and strengthened ground storey.

Previous research [22] suggests that the storey drift of masonry structures corresponding to the performance level of severe damage and collapse is 1/200 and 1/150, respectively. In this sense, provided that the deformation of the two story is uniform, both renovated structures have a higher energy dissipation capacity than the original structure prior to the collapse criterion with drift of 1/150.

4. Discussions

Fig. 13 shows that at the cracking stage the deformation of ground floor of W2 was smaller than that of the 2nd floor, and the lateral (or secant) stiffness of the ground floor was larger than that of the 2nd floor. However, the RC shear walls and the RC frame beam of the ground floor cracked earlier than the 2nd floor masonry walls under the action of overturning moment, as displayed in Fig. 7(b), weakening the structural stiffness of the ground floor, and thus the difference of the stiffness between the 1st and 2nd floor was reduced. This made the failure distribution of specimen W2 relatively uniform. Moreover, the RC shear walls had a larger deformation capacity and ductility compared with the masonry walls. Consequently, specimen W2 had a higher post-peak deformation capacity than that of W1.

On the other hand, the structural stiffness and cracking load of W3 were significantly improved by polymer mortar jacketing and RC frame. However, during the loading process from cracking to ultimate load stage, the secant stiffness of the 2nd floor decreased from 74.8 kN/mm to 15.79 kN/mm, and the one of the ground floor decreased from 97.24 kN/mm to 43.8 kN/mm, suggesting that the stiffness degradation of 2nd storey was faster than that of ground floor. This made the deformation concentrated on the 2nd floor masonry walls, thereby reducing the deformation capacity of W3.

Therefore, during the design of renovation and strengthening, it is necessary to make the lateral stiffness of the two storeys compatible to avoid the failure concentration. Moreover, over-strengthening the ground storey is not recommended.

5. Conclusions

In this paper, two renovation schemes of masonry structures were proposed to expand space through removing bearing walls and seismic strengthening. The schemes included (1) removing two bearing walls at the ground storey, adding two short-width reinforced concrete shear walls and enlarging the sections of original beams (namely, scheme 1) as well as (2) removing one bearing wall, enlarging the sections of original beams and columns to form a single-bay frame and retrofitting the adjacent wall with polymer mortar jacketing and reinforcement layer (namely, scheme 2). Then the original and the two renovated masonry structures were tested in cyclic loading to check the validity of the renovation techniques against seismic loads, and the main conclusions are as follows:

1) All the three specimens reached similar peak resistance and demonstrated hysteretic behaviour with pinching phenomenon. Both renovated structures had much larger structural resistance than the original structure after cracking and before peak resistance at a given displacement. Moreover, prior to the global drift of 1%, the energy dissipation capacity of renovated structure with scheme 1 and 2 was significantly and slightly larger than that of original structure. Thereafter, the two renovation schemes had no advantage in terms of energy dissipation.
2) Moreover, the global stiffness of the renovated structure using scheme 2 was twice that of the original structure and the renovated structure using scheme 1. The stiffness was degraded

sharply within the first global drift of 0.2%, and the in-cycle stiffness degradation was basically exacerbated with increasing lateral deformation after the global drift of 0.6%.

3) Renovation with scheme 1 significantly improves the post-peak deformation capacity (i.e., the difference of failure displacement and peak displacement) of the structure. However, the renovation scheme 2 downgrades the total structural deformation capacity due to large stiffness of the renovated storey, implying that the great difference of structural stiffness between the 1st and 2nd floor leads to the severe failure concentration phenomenon and the reduction of deformation capacity.
4) It is not economic and reasonable to excessively enhance the structural stiffness of the renovated storey as failure concentration at the upper storey eclipses the energy dissipation capacity contributed by the renovated and strengthened ground storey.

CRediT authorship contribution statement

Fang-fang Wei: Conceptualization, Writing - original draft, Funding acquisition. **You-hua Zhu:** Investigation, Formal analysis, Writing - original draft. **Jun Yu:** Supervision, Methodology, Writing - review & editing. **Yong-quan Wang:** Supervision.

Declaration of competing interest

The authors declare that they have no known competing financial interests or personal relationships that could have appeared to influence the work reported in this paper.

Acknowledgement

The work presented in this paper was funded by the National Natural Science Foundation of China (Grant No.51608168), Natural Science Foundation of Jiangsu Province of China (Grant No. BK20180073); the Fundamental Research Funds for the Central Universities (No. 2017B16014; 2019B12814), and Qinglan Project.

References

[1] K. Qian, B. Li, Effects of masonry infill wall on the performance of RC frames to resist progressive collapse, J. Struct. Eng. 143 (9) (2017), https://doi.org/10.1061/(asce)st.1943-541x.0001860 04017118.
[2] N. Eren, E. Brunesi, R. Nascimbene, Influence of masonry infills on the progressive collapse resistance of reinforced concrete framed buildings, Eng. Struct. 178 (2019) 375–394, https://doi.org/10.1016/j.engstruct.2018.10.056.
[3] J. Yu, Y.-P. Gan, J. Wu, H. Wu, Effect of concrete masonry infill walls on progressive collapse performance of reinforced concrete infilled frames, Eng. Struct. 191 (2019) 179–193, https://doi.org/10.1016/j.engstruct.2019.04.048.
[4] D. Jing, S. Cao, H. Guo, Application of steel plate masonry composite structure technology for underpinning of masonry walls, China Civ, Eng. J. 42 (5) (2009) 55–60, https://doi.org/10.15951/j.tmgcxb.2009.05.014.
[5] D. Perrone, E. Brunesi, A. Filiatrault, R. Nascimbene, Probabilistic estimation of floor response spectra in masonry infilled reinforced concrete building portfolio, Eng. Struct. 202 (2020) 109842, https://doi.org/10.1016/j.engstruct.2019.109842.
[6] Ö. Can, Investigation of seismic performance of in-plane aligned masonry panels strengthened with Carbon Fiber Reinforced Polymer, Construct. Build. Mater. 186 (2018) 854–862, https://doi.org/10.1016/j.conbuildmat.2018.08.028.
[7] R. Capozucca, Double-leaf masonry walls under in-plane loading strengthened with GFRP/SRG strips, Eng. Struct. 128 (2016) 453–473, https://doi.org/10.1016/j.engstruct.2016.09.042.
[8] M. Gams, M. Tomazevic, T. Berset, Seismic strengthening of brick masonry by composite coatings: an experimental study, Bull. Earthq. Eng. 15 (10) (2017) 4269–4298, https://doi.org/10.1007/s10518-017-0136-4.
[9] D. Dizhur, M. Griffith, J. Ingham, Out-of-plane strengthening of unreinforced masonry walls using near surface mounted fibre reinforced polymer strips, Eng. Struct. 59 (2014) 330–343, https://doi.org/10.1016/j.engstruct.2013.10.026.
[10] M. Shabdin, M. Zargaran, N.K.A. Attari, Experimental diagonal tension (shear) test of Un-Reinforced Masonry (URM) walls strengthened with textile reinforced mortar (TRM), Construct. Build. Mater. 164 (2018) 704–715, https://doi.org/10.1016/j.conbuildmat.2017.12.234.
[11] Q. Xu, H. Jiang, L. Zhu, G. Du, Experimental study of old brick masonry wall strengthened with steel-meshed cement mortar, China Civ, Eng. J. 42 (4) (2009) 77–84, https://doi.org/10.15951/j.tmgcxb.2009.04.016.
[12] Y. Lin, D. Lawley, L. Wotherspoon, J.M. Ingham, Out-of-plane testing of unreinforced masonry walls strengthened using ECC shotcrete, Struct 7 (2016) 33–42, https://doi.org/10.1016/j.istruc.2016.04.005.
[13] Y.-W. Lin, L. Wotherspoon, A. Scott, J.M. Ingham, In-plane strengthening of clay brick unreinforced masonry wallettes using ECC shotcrete, Eng. Struct. 66 (2014) 57–65, https://doi.org/10.1016/j.engstruct.2014.01.043.
[14] M.R. Maheri, M.K. Khajeheian, F. Vatanpour, In-plane seismic retrofitting of hollow concrete block masonry walls with RC layers, Struct 20 (2019) 425–436, https://doi.org/10.1016/j.istruc.2019.05.008.
[15] H.A. Khan, R.P. Nanda, D. Das, In-plane strength of masonry panel strengthened with geosynthetic, Construct. Build. Mater. 156 (2017) 351–361, https://doi.org/10.1016/j.conbuildmat.2017.08.169.
[16] X. Zhang, Q. Yue, X. Liu, Y. Yan, Experimental research on mechanical property of underpinnig structure in masonry wall, J. Build. Struct. 37 (6) (2016) 190–195, https://doi.org/10.14006/j.jzjgxb.2016.06.023.
[17] D. Cao, Q. Tan, W. Ge, B. Wang, Experimental study on flexural behaviours of composite component of concrete-masonry underpinning beams, J. Build. Struct. 35 (7) (2014) 145–152, https://doi.org/10.14006/j.jzjgxb.2014.07.018.
[18] S.J. Hardy, Design of steel lintels supporting masonry walls, Eng. Struct. 22 (6) (2000) 597–604, https://doi.org/10.1016/S0141-0296(99)00004-8.
[19] Ministry of Housing and Urban-Rural Development of the People's Republic of China (MOHURD), Code for Design of Masonry Structures, GB50003-2011, Beijing,China, 2011.
[20] Ministry of Housing and Urban-Rural Development of the People's Republic of China (MOHURD), Code for Seismic Design of Buildings, GB50011-2010, Beijing, China, 2010.
[21] MOHURD, Specification for Seismic Test of Buildings JGJ/T 101-2015, China Architechture and Building Press, Beijing, 2015.
[22] Q. Su, H. Xu, H. Wu, Y. Zhang, G. Liu, Research on inter-story displacement angle of brick masonry structures, China Civ. Eng. J. 46 (S1) (2013) 111–116, https://doi.org/10.15951/j.tmgcxb.2013.s1.041.